Inverse Saffman-Taylor Experiments with Particles Lead to Capillarity Driven Fingering Instabilities

Ilyesse Bihi,[1,2] Michael Baudoin,[1,*] Jason E. Butler,[2] Christine Faille,[3] and Farzam Zoueshtiagh[1,†]
[1]*Université Lille, CNRS, ECLille, ISEN, Université Valenciennes, UMR 8520–IEMN, F-59000 Lille, France*
[2]*Department of Chemical Engineering, University of Florida, Gainesville, Florida 32611, USA*
[3]*INRA, UR638, Villeneuve d'Ascq, France*
(Received 14 January 2016; published 12 July 2016)

Using air to displace a viscous fluid contained in a Hele-Shaw cell can create a fingering pattern at the interface between the fluids if the capillary number exceeds a critical value. This Saffman-Taylor instability is revisited for the inverse case of a viscous fluid displacing air when partially wettable hydrophilic particles are lying on the walls. Though the inverse case is otherwise stable, the presence of the particles results in a fingering instability at low capillary number. This capillary-driven instability is driven by the integration of particles into the interface which results from the minimization of the interfacial energy. Both axisymmetric and rectangular geometries are considered in order to quantify this phenomenon.

DOI: 10.1103/PhysRevLett.117.034501

The Saffman-Taylor instability [1–3] is a classical, interfacial instability that occurs when a low viscosity fluid displaces one of higher viscosity in a Hele-Shaw cell [4]. The instability generates a fingering phenomenon at the moving interface that leads to complex tree patterns. Aside from the beauty of the structures, the attention devoted to this instability can be attributed to its widespread relevance in applications such as flows in porous media [5–7], flame propagation [8,9], and growth of bacterial colonies [10]. The instability results from the decrease of the flow resistance as the fluid of lower viscosity replaces the more viscous fluid; the inverse situation, wherein a highly viscous fluid is pushed into a cell filled with a weakly viscous fluid, is stable. Despite the large number of investigations of interfacial instabilities, the displacement of air by a viscous fluid in the presence of particles has not been reported in the literature. Nevertheless, this case is of importance in cleaning processes when bacteria, spores, dust, or particles are present on surfaces.

Here, we demonstrate the formation of fingering patterns emerging from the injection of a liquid into a cell filled with air in the presence of microparticles on the walls. This corresponds to the reverse situation compared to the common Saffman-Taylor instability. This instability relies on the integration of partially wettable particles to the meniscus driven by the minimization of interfacial energy. A reverse Saffman-Taylor instability in the presence of surfactants has been previously reported in the literature by Chan *et al.* [11] and then by Fernandez *et al.* [12], but, in contrast to these studies, the fingers observed in our studies with particles are not limited in depth.

Air-water interfaces can induce strong capillary forces able to remove microparticles initially deposited on a wall surface. In nature, this phenomenon happens frequently when a raindrop falls on a lotus leaf. Because of the hydrophobicity of the surface and gravity, the water drop rolls off of the slanted leaf while also removing dust particles. This self-cleaning process is referred to as the "lotus effect" [13,14] and is of primary interest to a wide variety of industrial processes including tube [15,16] or microelectronic silicon wafer cleaning [17], separation of minerals in the mining industry [18], particle flotation [19], or even stabilization of bubbly liquids, foams, and emulsions [20–22]. Once the microparticles are removed from the surfaces, they are adsorbed and transported by the air-water interface. We show here how the presence of these particles can dramatically affect the stability of an interface.

This "particle-driven" fingering instability is first studied in a radial Hele-Shaw cell (see Fig. 1) which is constructed of two circular glass plates of radius 50 mm. They are centered and placed on top of each other at a separation distance of H, that was varied between 0.1 and 1 mm. The plates were cleaned prior to each experiment with isopropanol alcohol, distilled water, and acetone. Then, Rilsan (polyamide 11) particles with an average radius of 15 μm were sprinkled onto both glass surfaces to give a concentration C, as measured from microscopy images of the

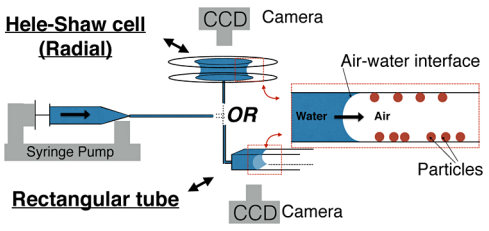

FIG. 1. Schematic of the experimental setup: water is injected into air using a syringe pump either between two parallel plates (radial Hele-Shaw cell) or inside a rectangular tube. Microparticles were deposited on the surfaces prior to water injection.

particle-covered plates. This concentration C corresponds to the ratio of the surface covered by the particles to the total surface. The uniformity of C was evaluated and is reported with each result. The particles have a density of 1.03 g/cm^2 and are hydrophilic ($S_p < 0$, $\theta_p = 71° \pm 3°$, with S_p the spreading parameter and θ_p the static contact angle between the particles and deionized water [16]). Water is injected into this cell through a hole drilled at the center of the bottom plate at constant flow rates Q (2, 20, 200 or 2000 ml/h) and the evolution of the liquid-air interface was recorded with a charge-coupled device camera. For the experiments described above, the capillary number, Reynolds number, and Bond number are defined, respectively, as $\mathrm{Ca} = \mu_l U/\gamma_{GL}$, $\mathrm{Re} = \rho_l U H/\mu_l$, and $\mathrm{Bo} = \rho_1 g H^2/\gamma_{GL}$, where ρ_l, μ_l, and γ_{GL} are the density, viscosity, and surface tension of the deionized water. Gravitational acceleration is g and the values of Bo range from approximately 10^{-3} to 10^{-1} depending on the plate separation. Both Ca and Re depend upon the velocity of the interface $U = Q/(2\pi r H)$, which is a function of the radius r. At the inlet where $r = 2$ mm, the maximum values are $\mathrm{Ca} \approx 10^{-3}$ and $\mathrm{Re} \approx 10^2$ and, at the outlet ($r = 40$ mm), the minimum values are $\mathrm{Ca} \approx 10^{-6}$ and $\mathrm{Re} \approx 10^{-4}$.

As fluid is injected between the plates, the air-water interface starts to expand radially. Microparticles encountered by the moving interface are captured and progressively cover the meniscus. When a critical radius r_c is reached, destabilization of the interface occurs and the formation of fingering patterns begins [see Fig. 2(a)]. To better understand this phenomenon, the critical radius was measured for different particle concentrations C, gap widths H, and flow rates (quantified by the capillary number Ca at the critical radius r_c); the data are shown in Fig. 2(b).

In the present case, the interface instability seems to occur once the meniscus is entirely covered with particles. To verify this hypothesis, we estimated theoretically the critical radius at which this happens from a simple balance of the surface occupied by the particles once they are collected by the meniscus and the space available on the meniscus as it expands radially (see Supplemental Material [23] for the detailed calculation). For wall contact angles α_E lying between 0 and $\pi/2$, the critical radius is predicted to be between

$$\underbrace{r_c/H = \frac{\phi\pi + \sqrt{\phi^2\pi^2 - 8C\phi}}{4C}}_{\text{for } \alpha_E = 0} \quad \text{and} \quad \underbrace{r_c/H = \frac{\phi}{C}}_{\text{for } \alpha_E = \pi/2}. \tag{1}$$

The measured value of the contact angle at the wall is $10° \pm 4°$ in the absence of the particles, but contaminants introduced with the particles may alter this value. In this formula, ϕ is the specific surface area of the particles on the interface, that is to say the fraction of the surface that the particles occupy on the meniscus due to their shape and arrangement, in close packing configuration, once the meniscus is entirely covered with particles. There is no reason for the particles to be organized in a specific way; thus, ϕ is equated with random packing of spheres on a flat surface: $\phi \simeq 0.8$ [25,26]. This value may slightly fluctuate depending on the exact shape and organization of the particles. Since we cannot visualize the particles' organization on the meniscus, the critical radius is estimated for values of the specific surface area lying between 0.7 and 0.8. Figure 2(b) shows that the calculation of r_c closely matches the experimental results at low capillary numbers ($\mathrm{Ca} < 10^{-4}$), when interfacial phenomena largely dominate the dynamical phenomena, supporting the hypothesis.

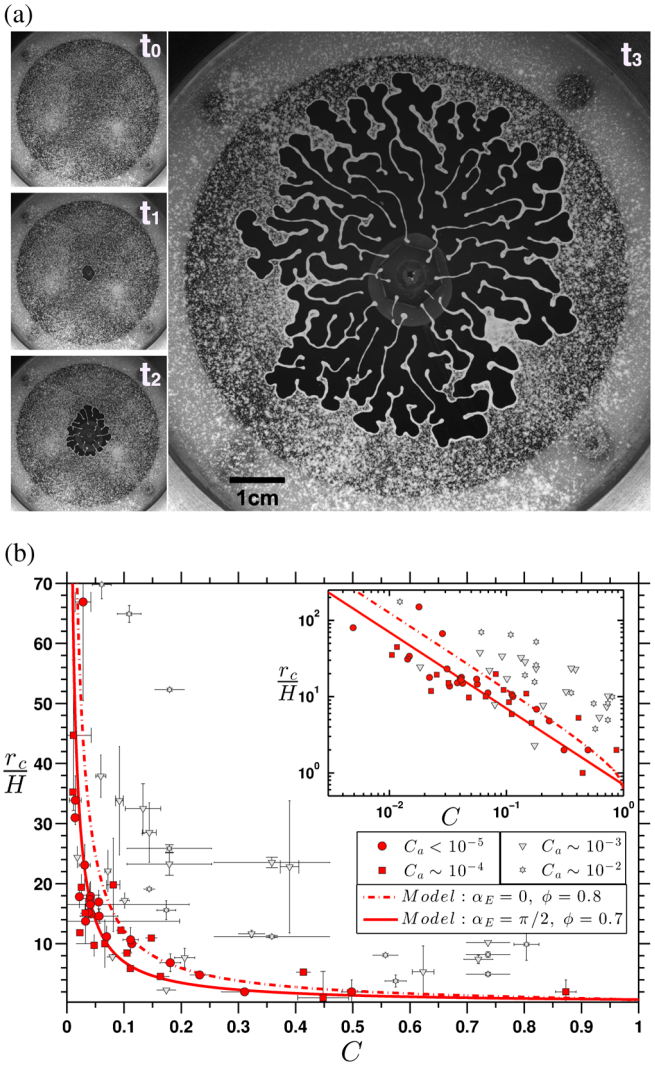

FIG. 2. (a) Images showing a time sequence of the interfacial instability in a radial Hele-Shaw cell with a plate spacing of 150 μm, $C = 0.78$, flow rate $Q = 200$ ml/h ($\mathrm{Ca} = 6.57 \times 10^{-4}$), and $[t_0, t_1, t_2, t_3 = 0, 3, 7, 31$ s]. (b) The critical radius at which the instabilities start in the radial Hele-Shaw cell. The horizontal error bars represent the standard deviation for the concentration with a confidence level of 96%. The vertical error bars represent the minimum and the maximum of the critical radius.

Indeed, it is well known [16,19,27] that hydrophilic particles are naturally collected by a liquid-air interface to minimize the interfacial energy. However, once the expanding interface becomes entirely covered by particles, integrating additional particles into the interface is not possible while also maintaining a purely radial growth. Instead, either the air-liquid interface will start expanding in a different way to incorporate new particles or the particles will remain in the gas or enter the liquid phase. The former case is always observed in the present experiments.

For concentrations $C \leq 0.8$, the integration of particles is achieved through the development of a fingering pattern that increases the interface to volume ratio as compared to the radial configuration. At very high particle concentrations ($C \geq 0.85$), the integration of particles is generally achieved through the deposition of a liquid film ahead of the meniscus, similar to what was observed previously in cylindrical tubes [16] and will not be further discussed here. For high capillary numbers, departure from our prediction is indicative of the role played by the fluid flow in the formation of the fingering patterns. Indeed, our model assumes that the evolution of the fingers is a quasistatic process solely driven by interfacial phenomena, which is no longer valid at higher capillary numbers.

We further investigated the structure of the patterns (finger widths and numbers, symmetry) as a function of the experimental parameters C, H, and Q (see Fig. 3). The width and number of fingers mainly depend on the plate separation distance H and the particle concentration C, while the symmetry of the patterns is mainly determined by the flow rate Q. At a low capillary number, some labyrinth patterns similar to those produced by the drainage of a granular-fluid system in two dimensional confinement [5] are formed. Indeed, the finger growth is solely driven by the particle collection. As long as the particles are uniformly distributed, no preferential direction of finger growth is observed. At a higher capillary number, the finger growth is essentially radial, similar to the viscous fingers produced by Saffman-Taylor instabilities, due to the increasing importance of radial viscous flow stresses.

The patterns formed in this radial Hele-Shaw configuration are relatively complex (see Fig. 3). There is an interplay between the number of fingers and their width and the fingers' progress intermittently and at varying rates (see Videos S1 and S2 [28]). To simplify this problem, we investigated the relation between the finger width L_D produced by this instability as a function of the particle concentration in a simpler geometry (rectangular borosilicate capillary tube of height $H = 0.40$ mm and width $W = 10H$), where the finger width is expected to be relatively constant. The inner walls were first degreased by sonication while suspended in acetone, then isopropanol, and finally in dichloromethane for five minutes each. Next, the tubes were dried under nitrogen flow and submerged in a freshly prepared piranha solution (sulfuric acid H_2SO_4 + hydrogen peroxide H_2O_2) at 100 °C for one hour. The channels were rinsed thoroughly with deionized water and dried in an oven at 120 °C for one hour. Then, the inner walls were covered by Rilsan (Polyamide11) particles by gently blowing them into the channel with an air jet. Water was injected through the tube at a constant flow rate $Q = 0.1$ ml/h, corresponding to a capillary number $\mathrm{Ca} = \mu_l Q/(\gamma_{GL} WH) = 2.38 \times 10^{-7}$, while recording the dynamics of the moving meniscus as described previously.

As water is injected into the tube, particles initially are collected by the meniscus at the relatively short times of t_o and t_1 as seen in Fig. 4(a). For longer times t_2 and t_3, an instability occurs and leads to the formation of a liquid finger as also observed in the radial Hele-Shaw geometry. Unlike the latter geometry, however, the fingers of water in the rectangular channel retain a uniform width L_D at each concentration C. The measurements of L_D, as given in

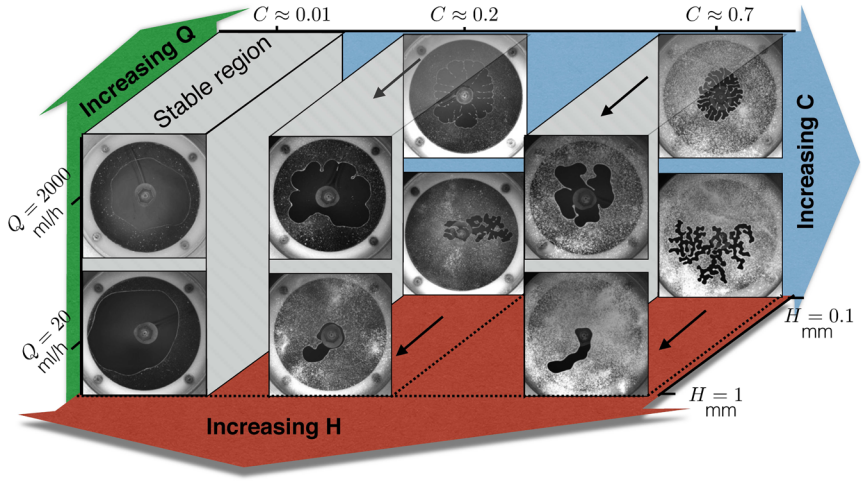

FIG. 3. Diagram of the different instability patterns as a function of the concentration of the particles C, the flow rate Q, and the gap between the plates H.

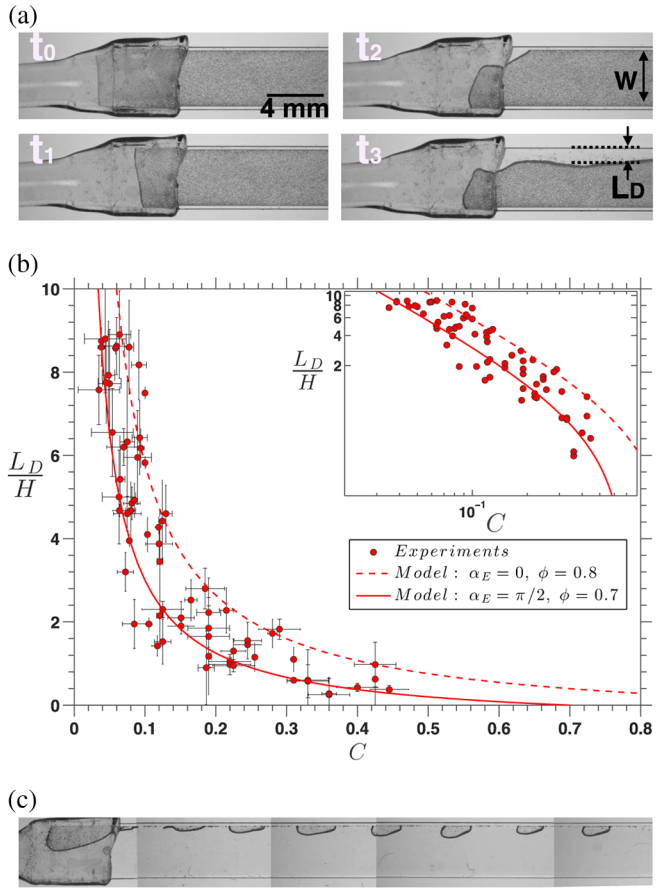

FIG. 4. (a) A time sequence of images showing the interface instability in a rectangular capillary tube with a particle concentration of $C = 0.3$ and capillary number $\mathrm{Ca} = 2.38 \times 10^{-7}$. The air appears dark gray and the water is light gray. (b) Measured and predicted finger width as a function of the concentration of the particles in the rectangular tube. The horizontal error bars represent the standard deviation for the concentration with a confidence level of 96%. The vertical error bars represent the minimum and the maximum of the finger width. (c) Semiarmored bubbles form when the finger width exceeds the width of the channel: $L_D/W > 1$.

Fig. 4(b), indicate an inverse relationship with the concentration C. It is interesting to note that when the finger width L_D exceeds the width W ($L_D/H \gtrsim 10$), the meniscus touches the opposite wall and semiarmored bubbles, attached to the walls, are formed periodically as seen in Fig. 4(c) and Video S3 [29].

As before, we suppose that the interface becomes unstable once covered by the particles and that the subsequent formation of fingers is driven by interfacial energy considerations. A theoretical liquid finger width, which corresponds to the limit size allowing all particles encountered by the meniscus to be captured, can be derived (see Supplemental Material [23]): $L_D = \phi\pi H/4C - H/2$ for a liquid-air-wall contact angle of $\alpha_E = 0$ and $L_D = \phi H/2C - H/2$ for a liquid-air-wall contact angle of $\alpha_E = \pi/2$. Comparisons of the measurements with the predictions for L_D are shown in Fig. 4(b) as a function of the particle concentration C for different model parameters α_E and ϕ, as these two parameters likely vary depending on the cleanliness of the surface and the distribution of the particles on the meniscus. The model captures the qualitative trends of the experimental data and the data are accurately bounded by the predictions of the limiting case of $\alpha_E = 0$ with $\phi = 0.8$, providing support for the idea that the finger width is simply fixed by an interfacial energy minimization process at low capillary numbers.

To conclude, we have demonstrated that the presence of partially wettable particles on the walls can dramatically affect the dynamics of a liquid that is injected into a Hele-Shaw cell filled with air. Generally, a fingering pattern forms, even though the displacement of air with a viscous fluid is typically stable, unlike the classical Saffman-Taylor instability. The destabilization of the interface occurs due to interfacial energy minimization, which requires that all particles intersected by the meniscus are collected. As a consequence, the critical radius at which the instability occurs and the width of the fingers can be calculated by simply balancing the space available on the meniscus with the area needed to accommodate additional particles encountered by the liquid-air interface during its motion.

We gratefully acknowledge the support from Marie Curie IRSES Fellowship No. 269207 entitled "Patterns and Surfaces" within the 7th European Community Framework Programme.

*michael.baudoin@univ-lille1.fr
†farzam.zoueshtiagh@univ-lille1.fr

[1] P. G. Saffman and G. Taylor, The penetration of a fluid into a porous medium or Hele-Shaw cell containing a more viscous liquid, Proc. R. Soc. A **245**, 312 (1958).
[2] E. Álvarez-Lacalle, J. Ortín, and J. Casademunt, Nonlinear Saffman-Taylor Instability, Phys. Rev. Lett. **92**, 054501 (2004).
[3] B. Levaché and D. Bartolo, Revisiting the Saffman-Taylor Experiment: Imbibition Patterns and Liquid-Entrainment Transitions, Phys. Rev. Lett. **113**, 044501 (2014).
[4] H. S. S. Hele-Shaw, The flow of water, Nature (London) **58**, 34 (1898).
[5] B. Sandnes, H. A. Knudsen, K. J. Maloy, and E. G. Flekkoy, Labyrinth Patterns in Confined Granular-Fluid Systems, Phys. Rev. Lett. **99**, 038001 (2007).
[6] B. Sandnes, E. G. Flekkoy, H. A. Knudsen, K. J. Maloy, and H. See, Patterns and flow in frictional fluid dynamics, Nat. Commun. **2**, 288 (2011).
[7] O. Johnsen, R. Toussaint, K. J. Maloy, and E. G. Flekkoy, Pattern formation during air injection into granular materials confined in a circular Hele-Shaw cell, Phys. Rev. E **74**, 011301 (2006).

[8] G. H. Markstein, in *Nonsteady Flame Propagation*, edited by G. H. Markstein (Pergamon Press, New York, 1964), Vol. 15, p. 103.
[9] P. Pelcé, *Dynamics of Curved Fronts* (Academic Press, Inc., New York, 1988).
[10] E. Ben-Jacob, O. Schochet, A. Tenenbaum, I. Cohen, A. Czirok, and T. Vicsek, Generic modeling of cooperative growth patterns in bacterial colonies, Nature (London) **368**, 46 (1994).
[11] C. K. Chan and N. Y. Liang, Observations of Surfactant Driven Instability in a Hele-Shaw Cell, Phys. Rev. Lett. **79**, 4381 (1997).
[12] J. Fernandez, R. Krechetnikov, and G. M. Homsy, Experimental study of a surfactant-driven fingering phenomenon in a Hele-Shaw cell, J. Fluid Mech. **527**, 197 (2005).
[13] J. Zhang, X. Sheng, and L. Jiang, The dewetting properties of lotus leaves, Langmuir **25**, 1371 (2009).
[14] C. Neinhuis and W. Barthlott, Characterization and distribution of water-repellent, self-cleaning plant surfaces, Ann. Bot. **79**, 667 (1997).
[15] S. Aramrak, M. Flury, and J. B. Harsh, Detachment of deposited colloids by advancing and receding air-water interfaces, Langmuir **27**, 9985 (2011).
[16] F. Zoueshtiagh, M. Baudoin, and D. Guerrin, Capillary tube wetting induced by particles: towards armoured bubbles tailoring, Soft Matter **10**, 9403 (2014).
[17] A. F. M. Leenaars and S. B. G. O'Brien, Particle removal from silicon substrates using surface tension forces, Philips J. Res. **44**, 183 (1989).
[18] Q. Min, Y. Duan, X. Peng, A. S. Mujumdar, C. Hsu, and D. Lee, Froth flotation of mineral particles: Mechanism, Drying Technol. **26**, 985 (2008).
[19] C. Huh and S. G. Mason, The flotation of axisymmetric particles at horizontal liquid interfaces, J. Colloid Interface Sci. **47**, 271 (1974).
[20] B. P. Binks, Particles as surfactants–similarities and differences, Curr. Opin. Colloid Interface Sci. **7**, 21 (2002).
[21] W. Ramsden, Separation of solids in the surface-layers of solutions and 'suspensions' (observations on surface-membranes, bubbles, emulsions, and mechanical coagulation).—Preliminary Account, Proc. R. Soc. London **72**, 156 (1903).
[22] B. P. Binks and T. S. Horozov, Aqueous foams stabilized solely by silica nanoparticles, Angew. Chem. **117**, 3788 (2005).
[23] See Supplemental Material at http://link.aps.org/supplemental/10.1103/PhysRevLett.117.034501 for a detailed calculation of the critical radius and the finger width, which includes Refs. [16,24,25].
[24] Z. Yao, Ph.D. thesis, Geometries in Soft Matter, Syracuse University SURFACE, Paper 125, 2012.
[25] S. Torquato, Nearest-neighbor statistics for packings of hard spheres and disks, Phys. Rev. E **51**, 3170 (1995).
[26] J. G. Berryman, Random close packing of hard spheres and disks, Phys. Rev. A **27**, 1053 (1983).
[27] J. Shang, M. Flury, and Y. Deng, Force measurements between particles and the air-water interface: Implications for particle mobilization in unsaturated porous media, Water Resour. Res. **45**, W06420 (2009).
[28] See Supplemental Material at http://link.aps.org/supplemental/10.1103/PhysRevLett.117.034501 for videos of the pattern formation during experiment in the Hele-Shaw cell.
[29] See Supplemental Material at http://link.aps.org/supplemental/10.1103/PhysRevLett.117.034501 for a video of the semiarmored bubbles formation during experiment.